

High Volumetric Energy Density Annealed-MXene-Nickel Oxide/MXene Asymmetric Supercapacitor

Qi Xun Xia^a, Jianjian Fu^a, Je Moon Yun^{*, b}, Rajaram S. Mane^b, and Kwang Ho Kim^{*,a,b}

^a*School of Materials Science and Engineering, Pusan National University, San 30 Jangjeon-dong, Geumjeong-gu, Busan 609-735, Republic of Korea*

^b*Global Frontier R&D Center for Hybrid Interface Materials, Pusan National University, San 30 Jangjeon-dong, Geumjeong-gu, Busan 609-735, Republic of Korea*

Email: kwhokim@pusan.ac.kr (K. H. Kim, Prof.)
[* yunjemoon@gmail.com](mailto:yunjemoon@gmail.com) (J. M. Yun, Dr.)

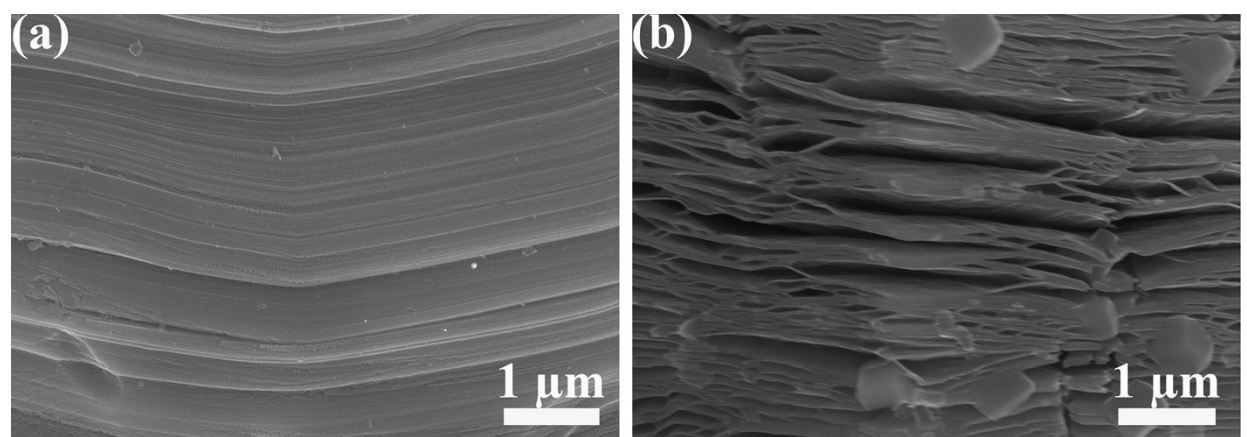


Figure S1. SEM images of the (a) as-obtained before HF treatment Ti_3AlC_2 MAX phase, and (b) after HF treatment $\text{Ti}_3\text{C}_2\text{T}_x$ MXene.

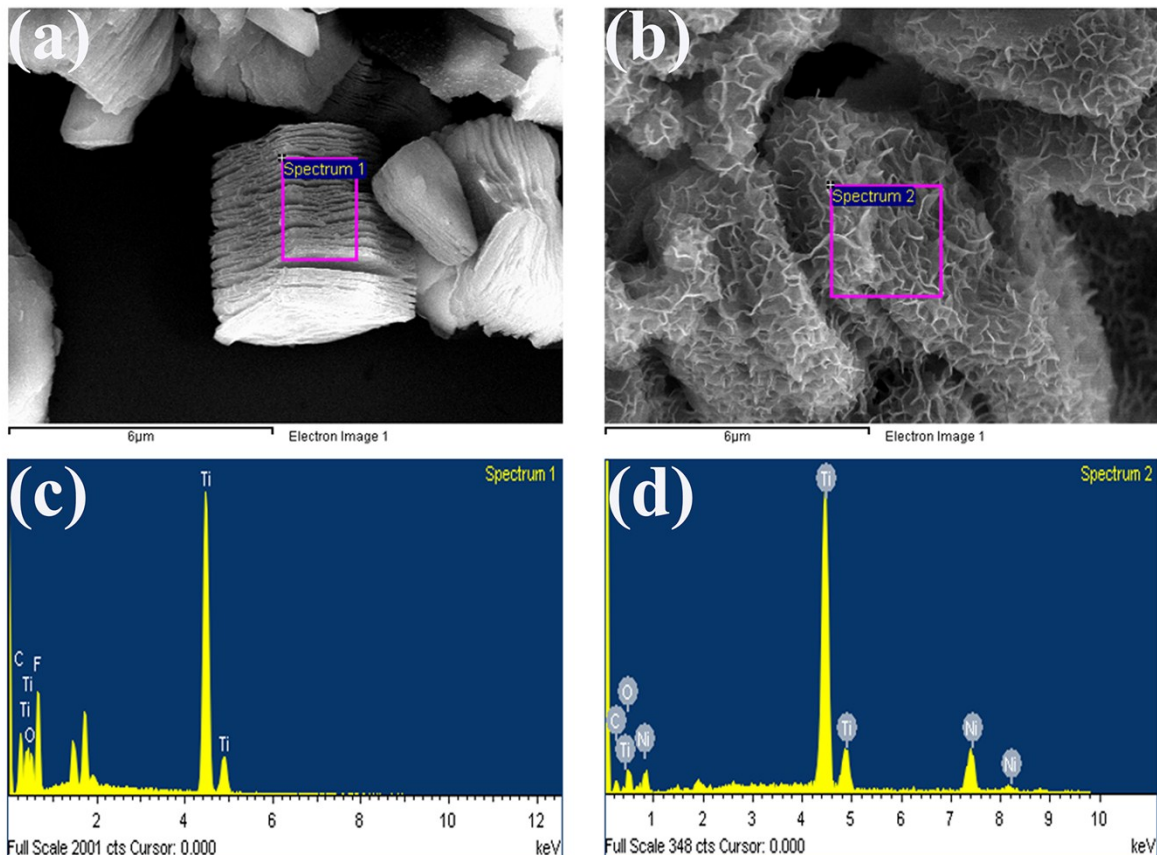


Figure S2. (a) SEM images of the $\text{Ti}_3\text{C}_2\text{T}_x$ MXene with corresponding selected-area EDX spectrum (c), and (e) corresponding elements content. (b) SEM images of the Ni-dMXNC with corresponding selected-area EDX spectrum (d), and (f) corresponding elements content.

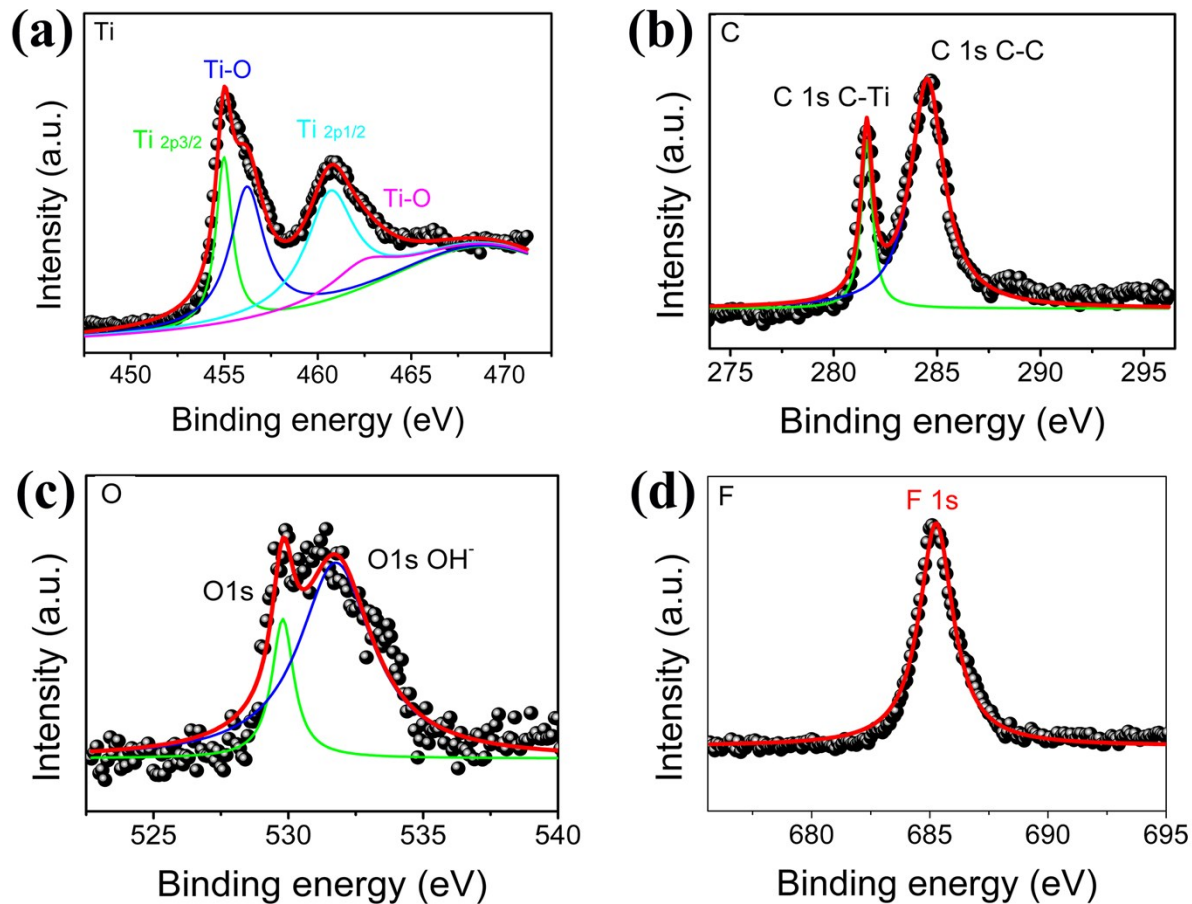


Figure S3. High-resolution XPS spectra (a) Ti 2p, (c) C 1s, (d) Ni 2p, (e) O 1s, and (f) F 1s spectra of $\text{Ti}_3\text{C}_2\text{T}_x$ MXene.

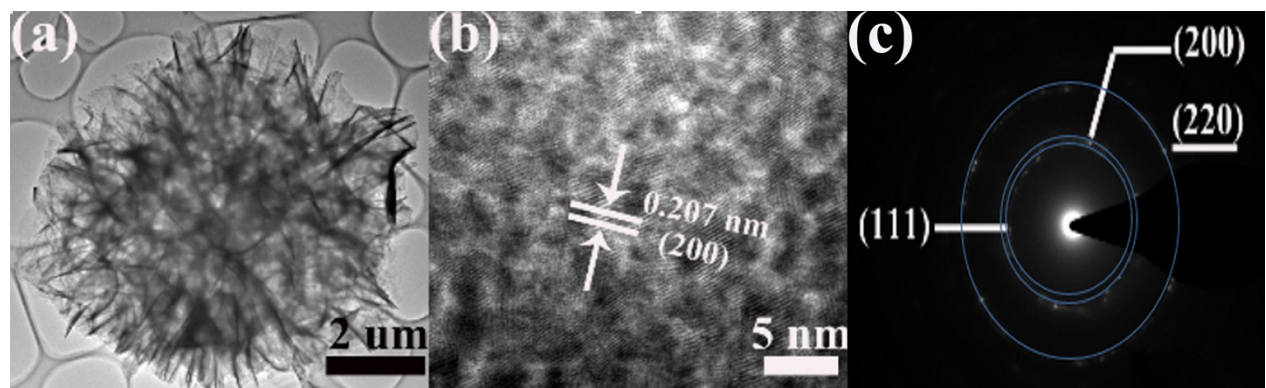


Figure S4. (a) Low magnification TEM image, (b) HRTEM image and (c) corresponding SAED pattern of the NiO nanosheets.

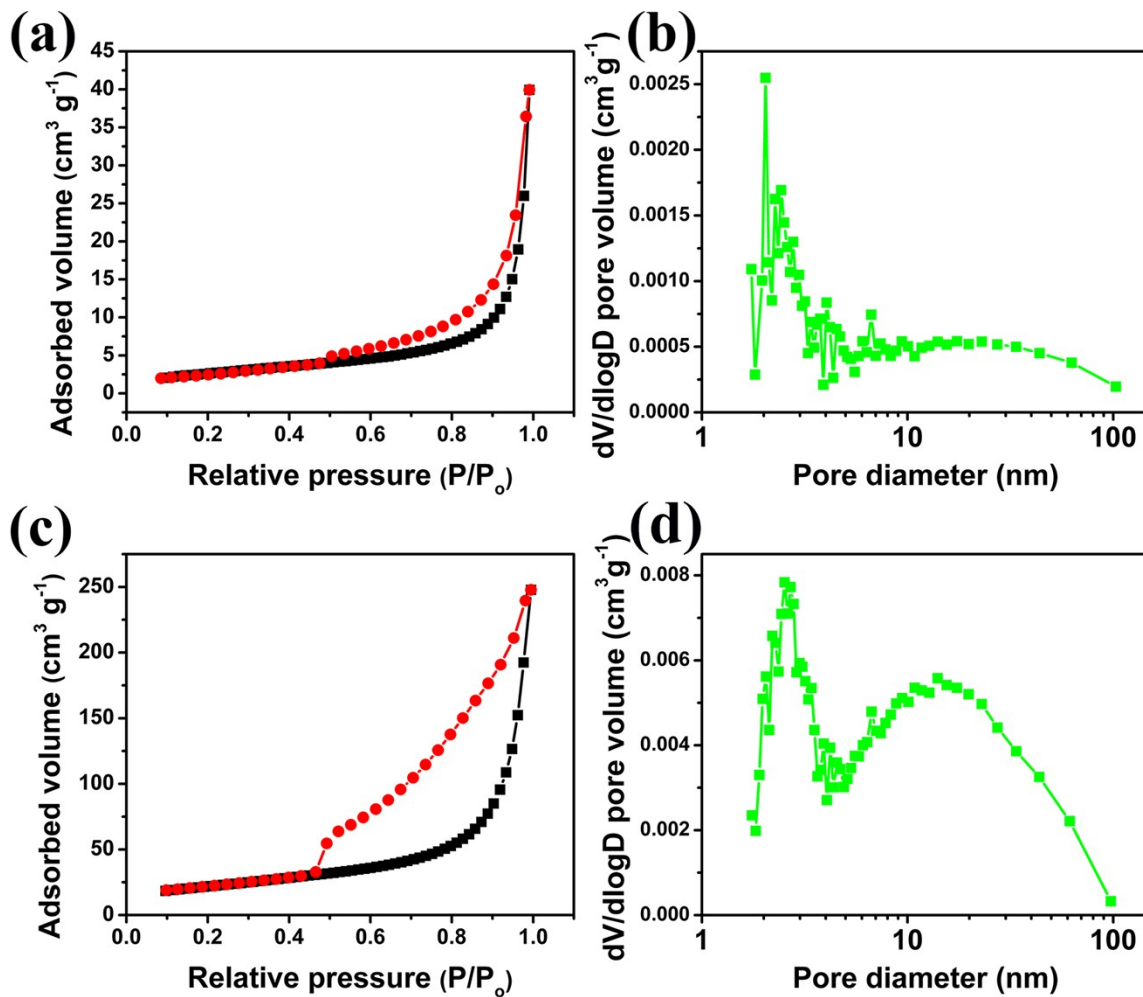


Figure S5. Pore structure of $\text{Ti}_3\text{C}_2\text{T}_x$ MXene and Ni-dMXNC (a) Nitrogen adsorption-desorption isotherms and (b) the BHJ pore-size distribution of the $\text{Ti}_3\text{C}_2\text{T}_x$ MXene; (c) Nitrogen adsorption-desorption isotherms and (d) the BHJ pore-size distribution of the Ni-dMXNC.

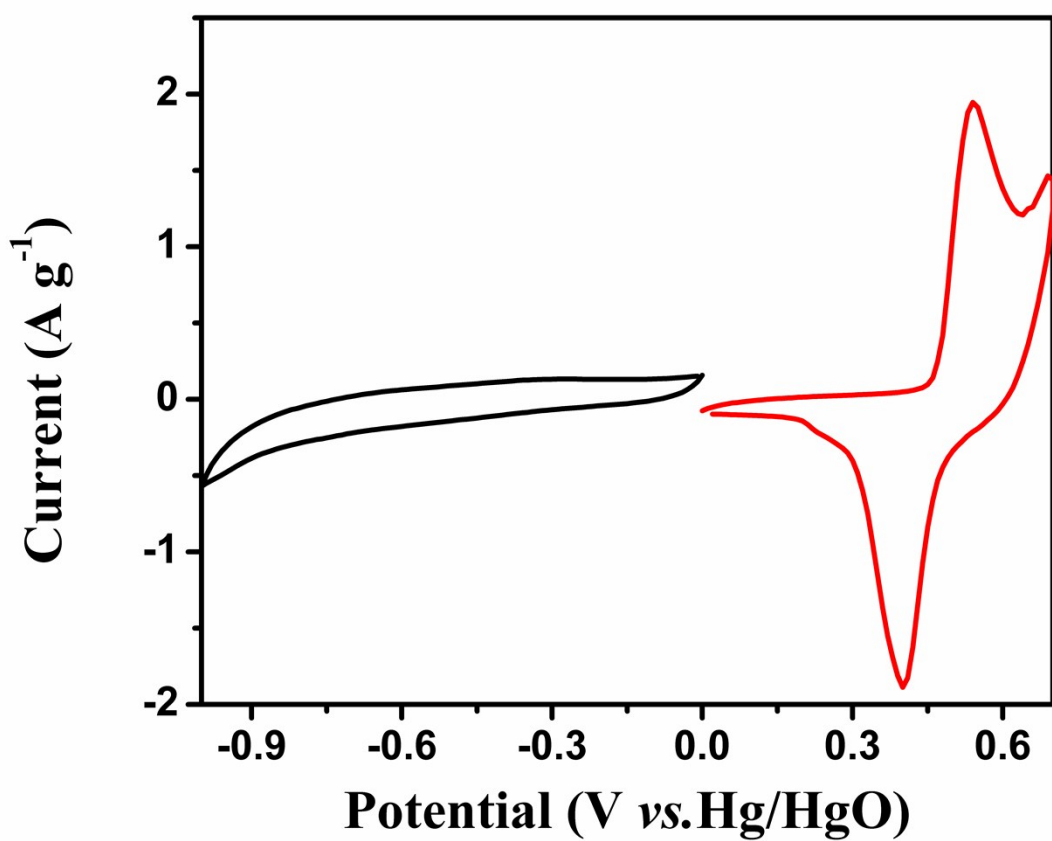


Figure S6. CV curves of the $\text{Ti}_3\text{C}_2\text{T}_x$ MXene electrodes in different potential range at scan rate of 10 mV s^{-1} .

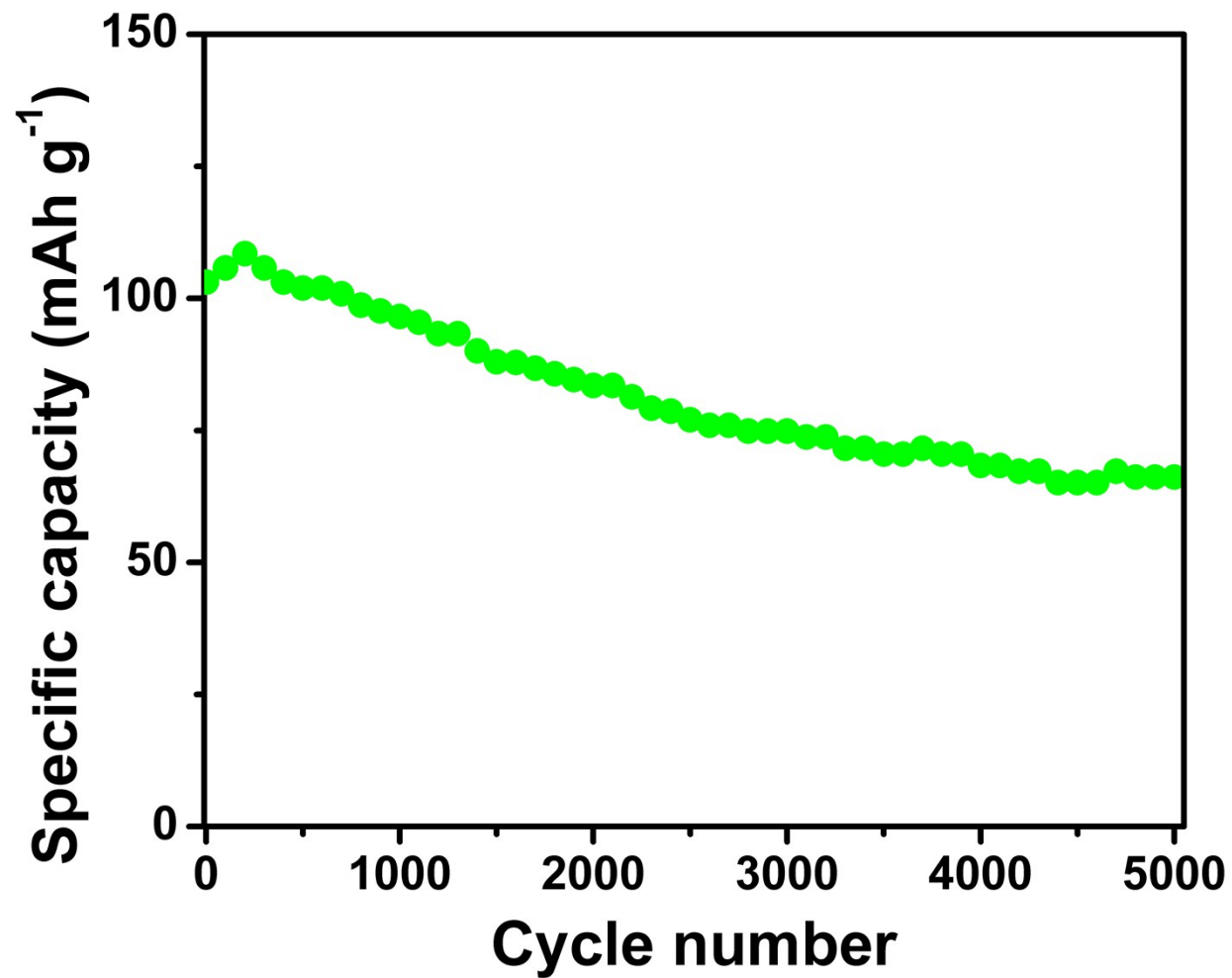


Figure S7. Cycling performance of the NiO electrode at a current density of 5 A g^{-1} .

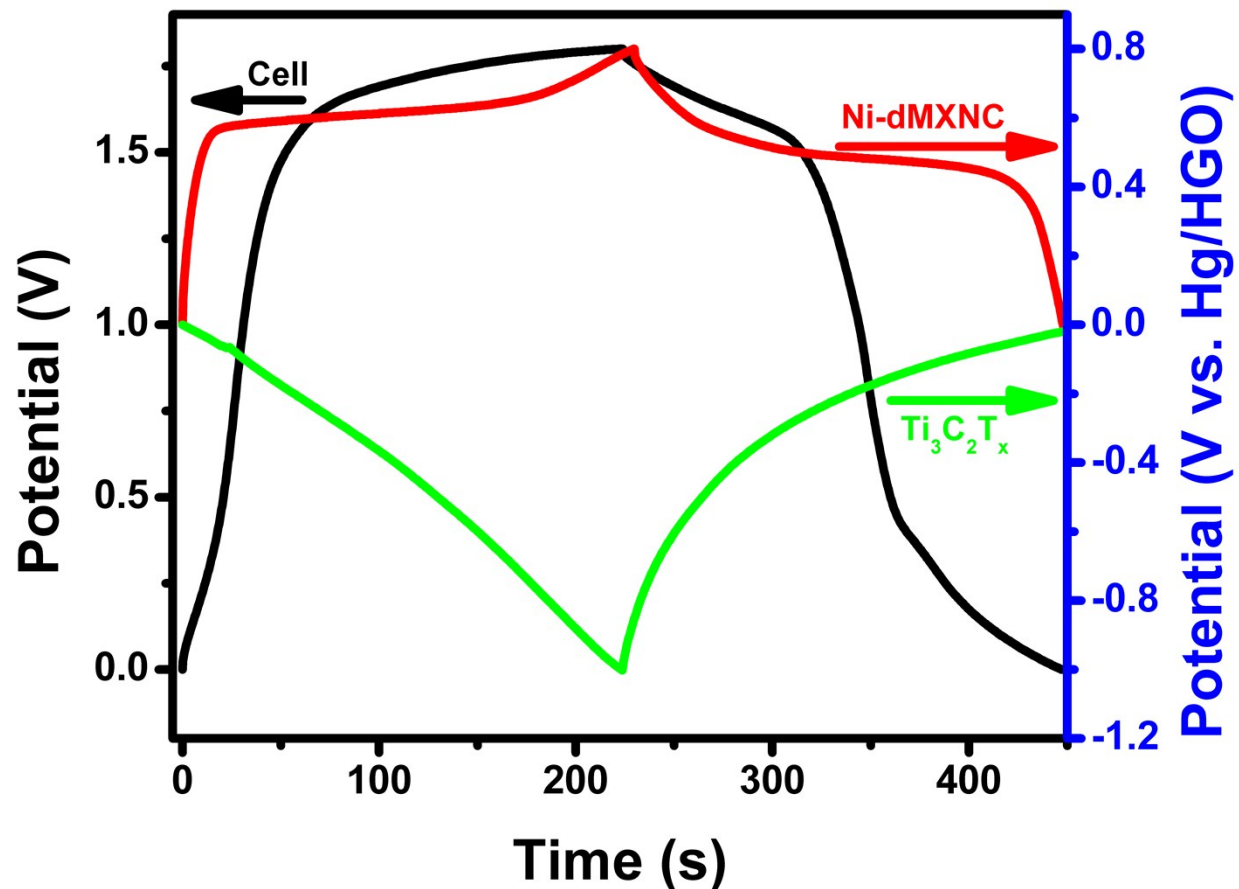


Figure S8. Galvanostatic charge-discharge curves of the asymmetric cell and the in situ tracked variation of the potential in each individual electrode.

Table S1. Resistivity of the $\text{Ti}_3\text{C}_2\text{T}_x$ MXene and Ni-dMXNC materials.

Sample	Resistivity (Ω/\square)	Resistivity ($\Omega \text{ m}$)
$\text{Ti}_3\text{C}_2\text{T}_x$	1.54E+4	6.76E+2
Ni-dMXNC	4.71E+3	3.30E+2

Table S2. Comparison of maximum gravimetric capacitance and volumetric capacitance of the reported MXene-based materials and the present work.

Positive electrodes	C_s (F g ⁻¹)	C_s (F cm ⁻³)	Electrolyte	Ref.
Ti ₃ C ₂ T _x		360 (2 mV s ⁻¹)	1 M MgSO ₄	[1]
Ti ₃ C ₂ T _x	53 (2 mV s ⁻¹)		0.05 M LiCl	[2]
Ti ₃ C ₂ T _x		49.6 (0.63 A cm ⁻³)	1 M H ₂ SO ₄	[3]
Ti ₃ C ₂	71.2 (2.5A/g)	119.8 (2.5A/g)	3 M KOH	[4]
Ti ₃ C ₂ -1.8	117 (2 mV s ⁻¹)		1 M KOH	[5]
Ti ₃ C ₂ T _x paper		442 (2 mV s ⁻¹)	1 M KOH	[6]
d-Ti ₃ C ₂		520 (2 mV s ⁻¹)	1 M H ₂ SO ₄	[7]
Ti ₃ C ₂ T _x -XAS	230 (1 mV s ⁻¹)		1 M H ₂ SO ₄	[8]
Ti ₃ C ₂ T _x hydrogel	70 (20 mV s ⁻¹)		Neat EMIM-TFSI	[9]
Ti ₃ C ₂ T _x clay	245 (2 mV s ⁻¹)	900 (2 mV s ⁻¹)	1 M H ₂ SO ₄	[10]
Ti ₃ C ₂ T _x MXene film	499 (2 mV s ⁻¹)	226 (2 mV s ⁻¹)	1 M H ₂ SO ₄	[11]
Ti ₃ C ₂ /CNT	85 (2 mV s ⁻¹)	245 (2 mV s ⁻¹)	1 M EMITFSI	[12]
d-Ti ₃ C ₂ T _x /CNT	193.5 (5 mVs ⁻¹)	393 (5 mVs ⁻¹)	6 M KOH	[13]
Sandwich Ti ₃ C ₂ T _x /CNT		390 (2 mV s ⁻¹)	1 M MgSO ₄	[1]
Sandwich Ti ₃ C ₂ T _x /rGO		435 (2 mV s ⁻¹)	1 M MgSO ₄	[1]
Sandwich Ti ₃ C ₂ T _x /MWCNT		321 (2 mV s ⁻¹)	1 M MgSO ₄	[1]
Nb ₂ CT _x /CNT paper	165 (5 mVs ⁻¹)	325 (5 mVs ⁻¹)	1 M LiPF6	[14]
Mo ₂ CT _x	196 (2 mV s ⁻¹)	700 (2 mV s ⁻¹)	1 M H ₂ SO ₄	[15]
Ti ₂ CT _x // Ti ₂ CT _x symmetric SC	51 (1 mV s ⁻¹)		30 % KOH	[16]
V ₂ CT _x /hard carbon	100 (0.2 mV s ⁻¹)	170 (0.2 mV s ⁻¹)	1 M NaPE6	[17]
Ni-dMXNC	273.2 (1 A g ⁻¹)	819.6 (1 A g ⁻¹)	1 M KOH	This work

References

1. M. Q. Zhao, C. E. Ren, Z. Ling, M. R. Lukatskaya, C. Zhang, K. L. Van Aken, M. W. Barsoum and Y. Gogotsi, *Adv. Mater.*, 2015, **27**, 339-345.
2. M. D. Levi, M. R. Lukatskaya, S. Sigalov, M. Beidaghi, N. Shpigel, L. Daikhin, D. Aurbach, M. W. Barsoum and Y. Gogotsi, *Adv. Energy Materials*, 2015, **5**, 1400815.
3. B. S. Shen, H. Wang, L. J. Wu, R. S. Guo, Q. Huang and X. B. Yanx, *Chin. Chem. Lett.*, 2016, **04**, 012.
4. Y. Gao, L. Wang, Z. Li, Y. Zhang, B. Xing, C. Zhang and A. Zhou, *J. Adv. Ceram.*, 2015, **4**, 130-134.
5. S. Y. Lin and X. Zhang, *J. Power Sources*, 2015, **294**, 354-359.
6. M. R. Lukatskaya, O. Mashtalir, C. E. Ren, Y. Dall'Agnese, P. Rozier, P. L. Taberna, M. Naguib, P. Simon, M. W. Barsoum and Y. Gogotsi, *Science*, 2013, **341**, 1502-1505.
7. Y. Dall'Agnese, M. R. Lukatskaya, K. M. Cook, P. L. Taberna, Y. Gogotsi and P. Simon, *Electrochim. Commun.*, 2014, **48**, 118-122.
8. M. R. Lukatskaya, S. M. Bak, X. Yu, X. Q. Yang, M. W. Barsoum and Y. Gogotsi, *Adv. Energy Materials*, 2015, **5**, 1500589.
9. Z. Lin, D. Barbara, P. L. Taberna, K. L. Van Aken, B. Anasori, Y. Gogotsi and P. Simon, *J. Power Sources*, 2016.
10. M. Ghidiu, M. R. Lukatskaya, M. Q. Zhao, Y. Gogotsi and M. W. Barsoum, *Nature*, 2014, **516**, 78-81.
11. M. Hu, Z. Li, H. Zhang, T. Hu, C. Zhang, Z. Wu and X. Wang, *Chem. Commun.*, 2015, **51**, 13531-13533.
12. Y. Dall'Agnese, P. Rozier, P. L. Taberna, Y. Gogotsi and P. Simon, *J. Power Sources*, 2016, **306**, 510-515.
13. P. Yan, R. Zhang, J. Jia, C. Wu, A. Zhou, J. Xu and X. Zhang, *J. Power Sources*, 2015, **284**,

38-43.

14. O. Mashtalir, M. R. Lukatskaya, M. Q. Zhao, M. W. Barsoum and Y. Gogotsi, *Adv. Mater.*, 2015, **27**, 3501-3506.
15. J. Halim, S. Kota, M. R. Lukatskaya, M. Naguib, M. Q. Zhao, E. J. Moon, J. Pitock, J. Nanda, S. J. May and Y. Gogotsi, *Adv. Funct. Mater.*, 2016, **26**, 3118-3127.
16. R. Rakhi, B. Ahmed, M. Hedhili, D. H. Anjum and H. N. Alshareef, *Chem. Mater.*, 2015, **27**, 5314-5323.
17. Y. Dall'Agnese, P. L. Taberna, Y. Gogotsi and P. Simon, *J. Phys. Chem. Lett.*, 2015, **6**, 2305-2309.